International Journal of Refractory Metals & Hard Materials 75 (2018) 153–162

Contents lists available at ScienceDirect

International Journal of Refractory Metals & Hard Materials

journal homepage: www.elsevier.com/locate/IJRMHM

Tensile properties of baseline and advanced tungsten grades for fusion applications

Chao Yin[a,b], Dmitry Terentyev[a,*], Thomas Pardoen[b], Anastasiia Bakaeva[a,c], Roumen Petrov[c], Steffen Antusch[d], Michael Rieth[d], Monika Vilémová[e], Jiří Matějíček[e], Tao Zhang[f]

[a] Structural Materials Group, Institute of Nuclear Materials Science, SCK•CEN, 2400 Mol, Belgium
[b] Institute of Mechanics, Materials and Civil Engineering, Université catholique de Louvain, 1348 Louvain-la-Neuve, Belgium
[c] Department of Electrical Energy, Metals, Mechanical constructions & Systems, Ghent University, 9052 Ghent, Belgium
[d] Karlsruhe Institute of Technology (KIT), Institute for Applied Materials, 76344 Eggenstein-Leopoldshafen, Germany
[e] Institute of Plasma Physics, The Czech Academy of Sciences, 18200 Prague, Czech Republic
[f] Institute of Solid State Physics, Chinese Academy of Sciences, 230031 Hefei, Anhui, China

ARTICLE INFO

Keywords:
Tungsten
Mechanical properties
Uniform elongation
Fusion

ABSTRACT

This work aims to establish a mechanical reference database of tungsten materials that are currently under assessment of their susceptibility to neutron irradiation. To obtain the mechanical properties, we performed a set of parametric tests using mini-tensile sample geometry and fracture surface analysis. Six different types of tungsten-based materials were assessed: two commercial grades produced according to ITER specifications in Europe and China - i.e., Plansee (IGP) and AT&M (CEFTR), and four perspective lab-scale grades. These are grades reinforced with particles of TiC, Y_2O_3, and ZrC (W1TiC, W2YO, and W0.5ZC, respectively) as well as fine grain structure W (FG). Tests were performed in the temperature range 150–600 °C, selected specifically to reveal the ductile to brittle transition temperature and mechanisms of full plastic deformation. Most of the materials showed onset of the ductile behavior at 300 °C, except FG and IGP (in transverse orientation) grades. High yield strength and ultimate tensile strength were recorded for CEFTR, W0.5ZC, and W1TiC at the maximum investigated temperature (600 °C), which can be considered as promising for performance in the high-temperature regime. The lowest threshold temperature for ductility was determined to be 200 °C registered for the W0.5ZC grade, CEFTR (in longitudinal orientation) grades, and IGP (in longitudinal orientation) grades, hence demonstrating its high potential for divertor applications.

1. Introduction

Nuclear fusion energy is considered as one of the alternative energy sources to replace fossil fuel in the future. Extraction of energy from the thermo-nuclear fusion reactor implies transfer of the kinetic energy of a neutron to a material thereby converting it into heat. Neutron irradiation in materials, potentially suitable for the nuclear fusion installations, insensibly degrades thermal, physical and mechanical properties thereby causing technological and safety concerns under prolonged operation [1]. Among different types of fusion reactor designs, Tokamak is one of the candidates, which has a high potential to be commercialized, and therefore it serves as main concept for DEMO (DEMOnstration Power Station) and ITER (International Thermonuclear Experimental Reactor) [2]. In both cases, tungsten is selected as primary candidate material for the heat exhaust system and divertor.

The operational conditions of DEMO are more demanding as compared to ITER as the first wall armor and divertor will experience longer pulses (> 2 h) and higher heat flux load (MW/m^2) [3], which will create thermal shock and fatigue phenomena along the operational period. Since tungsten (W) has high melting point, low erosion rate, high thermal conductivity, excellent thermal stress resistance, etc., it is selected as main candidate for the first wall armor and divertor applications [4]. However, high intrinsic ductile to brittle transition temperature (DBTT), neutron irradiation embrittlement, and recrystallization at high temperature imposes strict limits on the operational conditions of the plasma facing components to ensure its structural integrity.

Currently, EUROfusion consortium carries a large scale campaign to investigate the thermo-mechanical properties of baseline commercial tungsten and its advanced grades to account for the impact of neutron irradiation to make a step forward towards development of plasma-facing components sufficiently tolerant to neutron irradiation [5]. The

* Corresponding author.
E-mail address: dterenty@sckcen.be (D. Terentyev).

https://doi.org/10.1016/j.ijrmhm.2018.04.003
Received 12 February 2018; Received in revised form 3 April 2018; Accepted 7 April 2018
Available online 10 April 2018

mechanical properties of the commercial tungsten in non-irradiated state, produced by hot rolling/forging (e.g. produced by Plansee and ALMT companies), have been studied earlier in Refs. [6–11] including investigation of the effect of texture, annealing and cold-rolling processing. Overall, it is agreed that successful application of W in fusion reactors will be determined by a best compromise between reduced DBTT and enhanced fracture toughness as well as high recrystallization temperature. For that purpose, advanced W-based grades are under development to improve low- and high-temperature performance. For example, particle-reinforced tungsten and reduced grain size material can suppress the grain growth, improve the strength of grain boundary as well as fracture toughness of the material, and reduce DBTT (see reviews [12,13]). Fibre-reinforced tungsten allows one to overcome the intrinsic brittleness of tungsten and its susceptibility to embrittlement induced under operation, as W fibers arrest and deflect the propagating cracks (see e.g [14,15].). By dedicated alloying with zirconium-carbon (ZrC) nano-sized particles as well as by applying the powder metallurgical process, it was possible to reduce the free oxygen occupying grain boundaries and successfully fabricate bulk plate of W-0.5wt.%ZrC alloy [16]. Preliminary mechanical and high heat flux (HHF) assessment demonstrated that this material exhibits as low DBTT as 100 °C and sufficiently withstands HHF loads up to the power density of 0.66 GW/m^2 [16], simulated by electron beam. Next step is thus to investigate the impact of the neutron damage. As of now, there is a number of perspective lab-scale tungsten grades with improved mechanical properties whose performance under neutron irradiation is yet to be explored.

This work is dedicated to the systematic characterization of tensile properties and fracture surface of the several above discussed grades in non-irradiated state, selected for screening of the neutron irradiation impact. The samples are systematically fabricated, tested and inspected using the same lab equipment to provide one-to-one comparison. The same sample geometries are used to investigate the effect of neutron irradiation, which is currently being performed in BR2 reactor, Belgium. In order to assist the analysis of the impact of neutron irradiation, this research focuses on mechanical properties in the low-temperature range (< 600 °C), where the irradiation induced embrittlement is considered to play a crucial role.

2. Experimental

2.1. Materials

Six types of materials were studied in this work. The W grades were selected in accordance with the most recent advances in the development of W for DEMO applications. Two commercial grades were produced in Europe and China: Plansee ITER specification W (IGP) and AT &M ITER specification W (CEFTR), respectively. Four R&D grades were developed, respectively, by Karlsruhe Institute of Technology in Germany (two particle reinforced tungsten products), by Institute of Plasma Physics in Czech Republic, and Institute of Solid State Physics in China: W-1 wt% TiC (W1TiC), W-2 wt% Y_2O_3 (W2YO), Fine Grain W (FG), and W-0.5 wt% ZrC (W0.5ZC). The main elements of the chemical composition of those grades are reported in Table 1.

Three grades (IGP, CEFTR, and W0.5ZC) were produced by powder metallurgy and normalized by forging or rolling. The double-hammering was applied for IGP, and rolling for CEFTR and W0.5ZC grades. The manufacturing process of W0.5ZC, which is developed by Chinese Academy of Sciences, also introduced thermal mechanical treatment (TMT) to reduce the grains size [16]. The two particle reinforced tungsten products (W1TiC and W2YO) were manufactured by powder injection molding (PIM). Finally, the FG products were manufactured by spark plasma sintering (SPS) processing.

To provide a quick glance at the variety of the microstructure, we performed SEM-EBSD analysis. The maps, which were mapped by Bruker Quantax software, reported in Fig. 1 indicate the morphology and size of grains (reported in Table 1; analyzed and calculated by MTEX). IGP and CEFTR show strong texture with elongated grains parallel to the rolling direction. As a result, IGP has carrot-like grains, and CEFTR has plate-like grains. W0.5ZC also shows crystallographic texture but with the nearly equiaxed grains, which is apparently the result of TMT. Since normalization forging or rolling was not applied to the advanced grades, they all have equiaxed grains. Among the selected R&D materials, W0.5ZC has the smallest grains. The commercial IGP and CEFTR grades have comparable grain size.

2.2. Material testing procedures

Uniaxial tensile tests were performed on small dog-bone shaped specimens, as shown in Fig. 2. The overall length of the specimens is 16 mm with a gauge length of 5.2 mm and an effective cross section of 2.4 mm2 (1.6 mm × 1.5 mm) or 2.88 mm2 (1.6 mm × 1.8 mm). Moreover, the gauge length to width ratio of was 3.25, which is close to the ASTM standard value (being 4). The thickness of the specimen will not influence the mechanical properties if the grain size is smaller than ≈1/10 of the specimen thickness such that each cross-section slab is being a representative volume element [17,18]. According to the EBSD analysis, all selected products have grain size smaller than 100 μm. Thus, the cross-section contains at least hundreds of grains making the response of the material to be representative. Moreover, for the IGP product, it has been confirmed by the tensile tests that the mechanical response is equivalent (within the error of the measurement) using both 2.4 and 2.88 mm^2 cross-section in the bounds of the test temperatures. Moreover, according to the work by Zhao, et al. [19], the effect of thickness on R.A.% is negligible when the thickness of specimen is larger than 1 mm.

Given that the commercial products exhibit the texture, two sets of samples with longitudinal (L) and transverse (T) orientation were investigated for IGP and CEFTR, as shown schematically in Fig. 3. For all the studied materials, the samples were cut by electric discharge machine using the wire of 20–50 μm and no special treatment was applied to the surface.

The tests were conducted within the temperature range from 150 to 600 °C to comply with the critical need to clarify the onset of ductility in W for the water-cooled design of DEMO divertor. The tests were performed using a 50 kN load cell. To align the specimen, a preloading of 100 N or 200 N was applied. The selection of preloading force was determined on the basis of the yield strength of the materials: the higher the yield strength the higher preloading force is. The tests were performed at a constant displacement rate of 0.2 mm/min, corresponding to the strain rate of 6.41 × 10^{-4} s^{-1}. In order to reduce the uncertainty of the cross-head displacement, the test bench was

Table 1
Composition and grain size of the tested materials observed from ND; the equivalent medium diameter is defined as the equivalent diameter of grains that have 50% cumulative area fraction.

Materials	IGP	CEFTR	FG	W1TiC	W2YO	W0.5ZC
Composition	Pure W (> 99.97 wt%)	Pure W (> 99.94 wt%)	Pure W (> 99.7 wt%)	99 wt% W + 1 wt% TiC	98 wt% W + 2 wt% Y_2O_3	99.5 wt% W + 0.5 wt% ZrC
Equivalent medium diameter (μm)	87.44	60.28	9.36	7.76	7.32	6.66

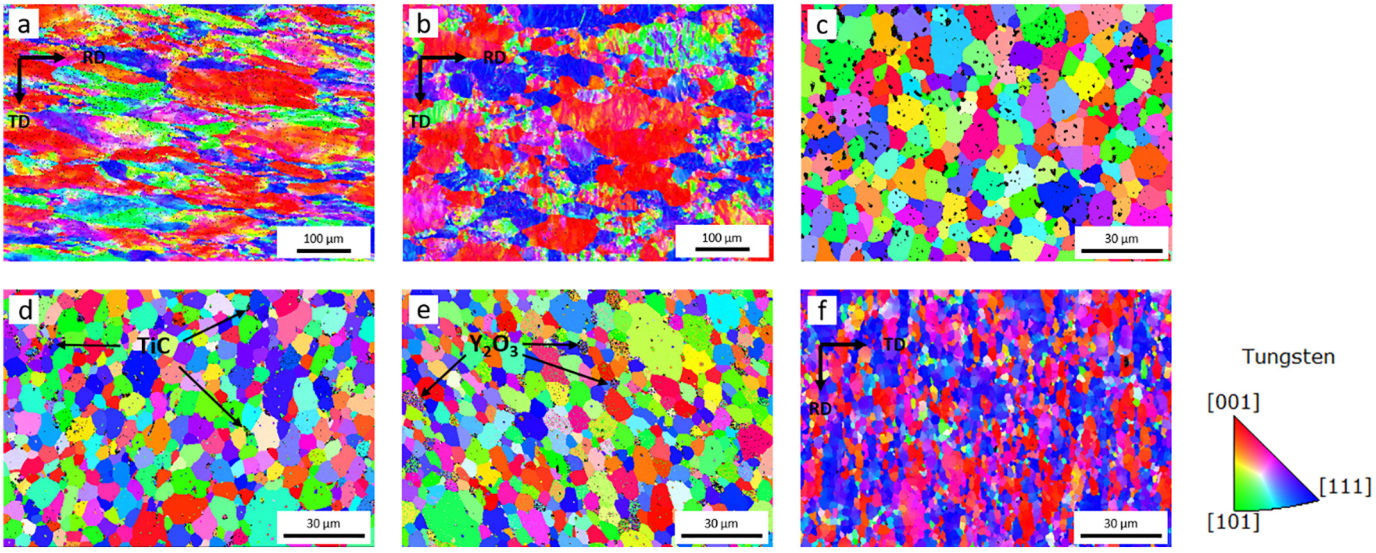

Fig. 1. Normal direction (ND) Inverse pole figure (IPF) of baseline and advanced W; (a) IGP; (b) CEFTR; (c) FG; (d) W1TiC; (e) W2YO; and (f) W0.5ZC.

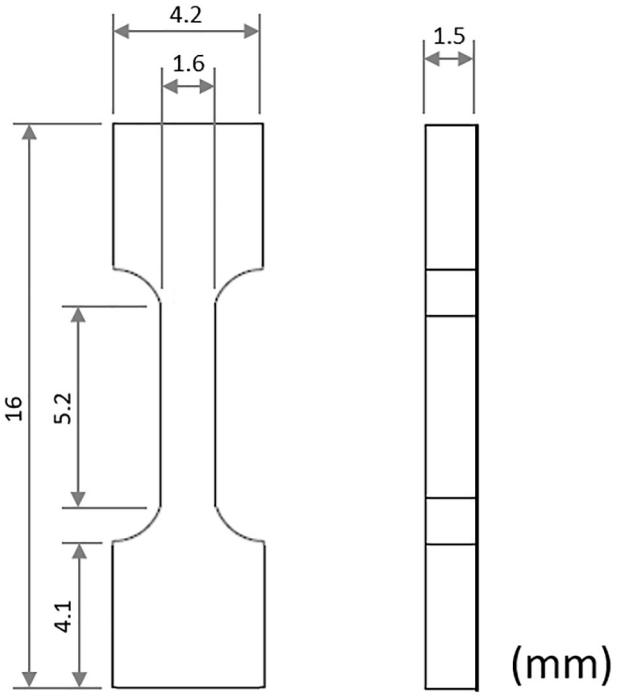

Fig. 2. Sketch of small dog-bone shaped specimens.

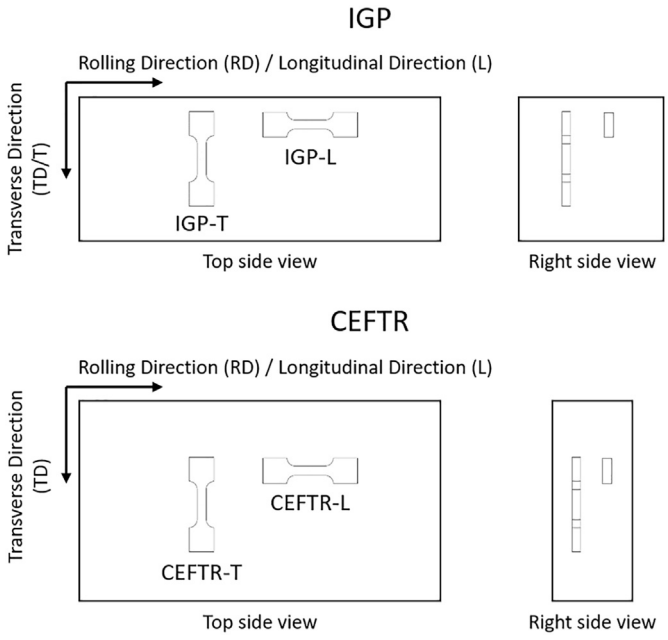

Fig. 3. Sample orientation.

calibrated and qualified according to the industrial ASTM standard prior to start of the measurements. The precise true strain will not be discussed in this work because small size testing techniques (SSTT) requires advanced methodology to measure strain (or even its distribution in the gauge section) [19,20].

After the tensile test, the fracture surface was investigated by scanning electron microscopy (SEM; JEOL6610 – 15 kV, spot size of 50 with secondary electron detector), and the initial microstructures were analyzed by electron back-scattered diffraction (EBSD; Bruker Quantax). The characterization methods and sample geometry are exactly the same as those to be used for post irradiation analysis, thus the current data and approach will establish the reference database.

In order to compensate for the influence of the machine compliance, the elastic region of stress-strain curve of pure W was calibrated by the known elastic moduli [21]; and for the particle reinforced W, the elastic region was adjusted by Halpin-Tsai equation, which describes the change of elastic modulus after introducing additional particles into matrix [22].

The definition of mechanical properties is described as follows. Yield strength (YS) is the engineering stress, which is measured at 0.2% of plastic deformation followed after the linear elastic deformation. Ultimate tensile strength (UTS) is the highest engineering stress measured, and the sample elongation at UTS point is defined as the uniform elongation. Fracture strength (Fstrength) is the true stress at the point of the fracture. Fracture strain (Fstrain) is the true strain at the point of the fracture, which is determined by the cross-area of the gauge before test and the smallest cross-area of gauge of the fractured sample.

3. Results

3.1. Strength and ductility

As shown in Fig. 4 and Fig. 5 c, the uniform elongation of W1TiC,

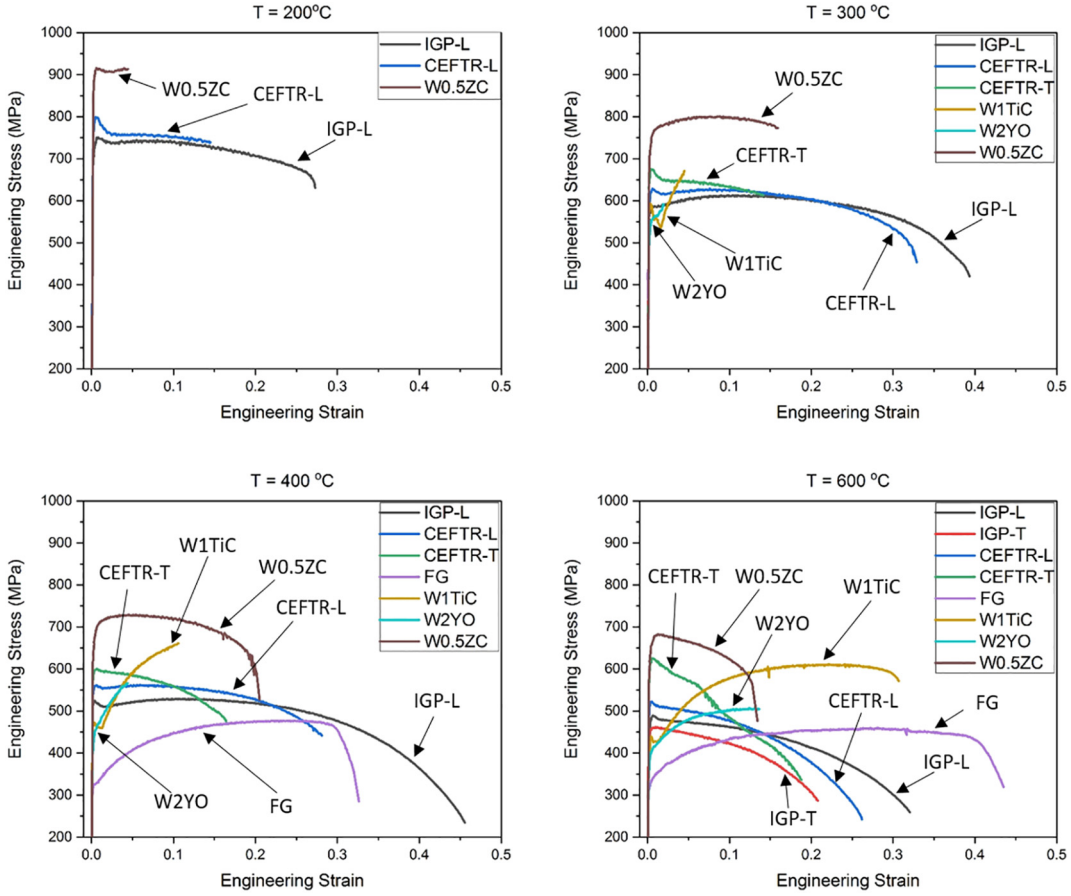

Fig. 4. Stress-strain curve of baseline and advanced W.

W2YO and FG increases with raising the temperature and W1TiC shows quite large value at 600 °C. Although FG also has a considerable uniform elongation, its UTS is lower as compared to other tested materials, and increasing the temperature does not lead to any substantial improvement. The uniform elongation of FG is practically independent of test temperature.

The stress-strain diagram for W0.5ZC differs from all other tested materials. Even though this material has extraordinary ductility below 300 °C, the uniform elongation at 400 °C and above is reduced drastically appearing the early necking deformation. However, this material preserves high YS and UTS in the whole studied temperature range.

All the tested materials exhibit similar trends, namely both YS and UTS are reduced with increasing the test temperature (see Fig. 5 a and b). Depending on the particular grade, the reduction follows either an exponential or linear trendline.

W0.5ZC shows the highest YS and UTS among all other advanced W grades in the whole temperature range. Comparison of IGP and CEFTR products (i.e. baseline commercial materials) reveals that AT&M grade has a higher YS and UTS. Moreover, as it will follow, the texture, grain orientation and shape, will also affect the strength of materials, for example, baseline W CEFTR-T had higher strength than CEFTR-L at all tested temperatures.

In order to compare the ductility and strength of the materials, UTS and uniform elongation were plotted in the same diagram (see Fig. 5 c). A combination of high strength and large uniform elongation indicates a material with high toughness and better fatigue resistance, which can also be quantified by calculating the product of both these value (see iso-values). The UTS variation on that figure could also serve as representation of the impact of testing temperature, since the UTS is inversely proportional to the test temperature for these materials. For commercial tungsten, both IGP and CEFTR grades show similar results, but IGP-L appears to have a larger uniform elongation, which indicates that IGP-L has a better ductility in terms of resistance to plastic localization.

The fracture properties quantified by the FStrength and by the Fstrain are plotted in Fig. 5 d. As one can see, the baseline W indicates a better fracture resistance compared to advanced W. The IGP-L has the highest FStrength and the largest Fstrain among the other grades. Even though the FStrength of IGP-L dropped strongly at 600 °C, the FStrength is still higher compared to the results obtained for other grades. The FStrength of CEFTR, for both L and T orientations, remains nearly constant over the whole temperature range, without dropping below 700 MPa. On the other hand, the FStrength and Fstrain measured for the advanced W appear to be rather low suggesting poor fracture resistance, at least in the range of tested temperature.

3.2. *Delamination fracture*

Microstructure analysis by SEM shows partial delamination of the fracture surface of IGP-L and CEFTR-L samples (tested at 300 °C) where the crack initiated on the down-left corner and upper two corners, respectively (see Fig. 6). The fracture surface of the IGP sample, tested at 400 °C and above for L-orientation, and tested at 600 °C for T-orientation, contains the delaminated fibers that are parallel with the RD. These features are apparently being related to the elongated grains that can be seen on EBSD maps. On the other hand, the delamination of CEFTR-L and –T oriented samples occurs along the TD-RD plane (see Fig. 6) and the grains show plastic deformation with elongated grains and dimples (see Fig. 7) at the test temperature exceeding 400 °C.

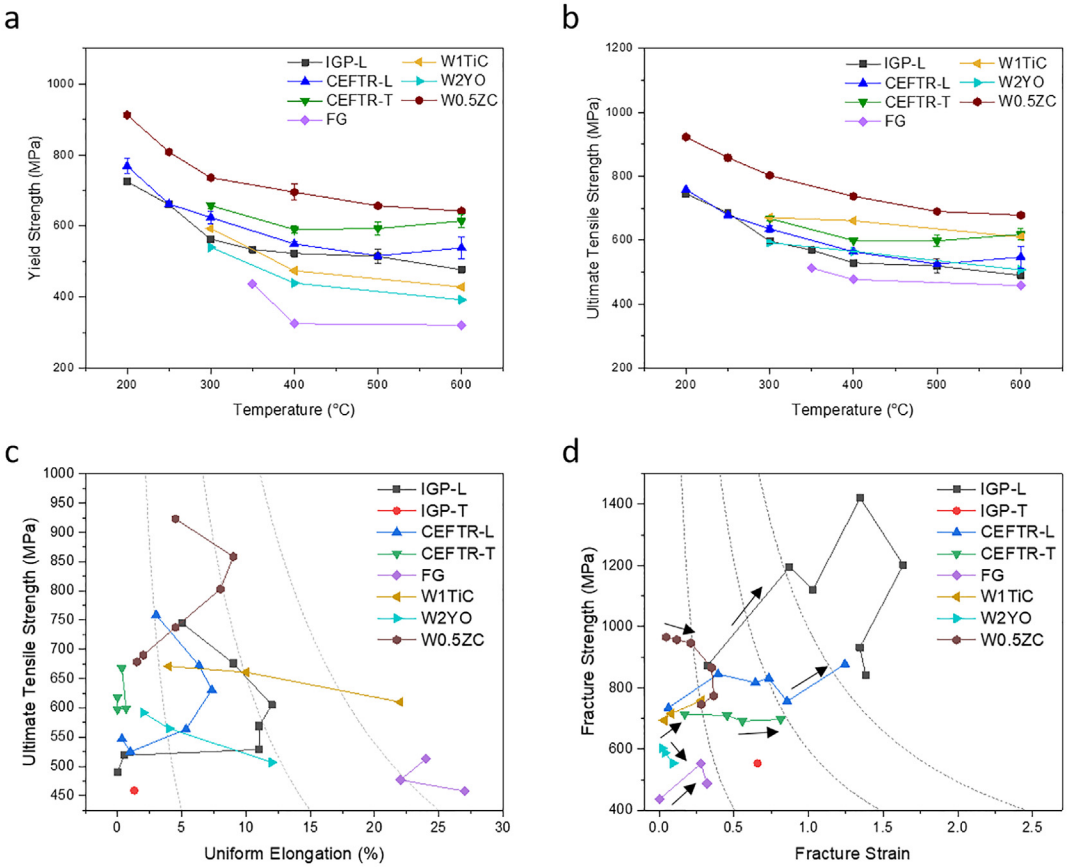

Fig. 5. Comparison of the mechanical properties of baseline and advanced W as a function of test temperature; (a) YS; (b) UTS; (c) UTS vs. uniform elongation; (d) Fracture strength vs. fracture strain, the arrows indicate the trend of increasing test temperature.

3.3. Transgranular and intergranular fracture

At 300 °C, the majority of the fracture surface of IGP-L and CEFTR-L appears to have features of the transgranular fracture (see Fig. 7). It indicates that both materials display strong adhesion between grains. For the T-orientated samples of both baseline W products, the fracture surface indicates the presence of both intergranular and transgranular fracture with a fraction close to 50/50. At 400 °C, the IGP-T sample still shows both brittle fracture features. The surface of IGP grade displayed in Fig. 7 corresponds to the stress-strain curve in Fig. 4, which proves that the IGP-T fractures in brittle manner up to 400 °C.

The grades showing the best mechanical properties have flatter (as compared to the delaminated samples) fracture surface covered with micro-dimples, which might be initial pores or left-out of particles, except for the W0.5ZC grade (see Figs. 6 and 7). The delamination fracture surface is observed only on the W0.5Zsample tested at 300 °C. The FG, W1TiC, and W2YO materials exhibit intergranular fracture at 300 °C. However, the fracture surface of the FG and W1TiC also contains a small fraction of transgranular fracture. At 400 °C, a part of the fracture surface of the FG exhibits dimples and a signature of the grain deformation hence it starts to show large elongation. These dimples indicate point to the ductile fracture mechanism operating via nucleation, growth and coalescence of voids. On the other hand, the fracture surface of the W1TiC and W2YO grades, tested at 400 °C, remains the same as at 300 °C. Finally, at the highest test temperature i.e. 600 °C, the evidence of brittle fracture is no longer observed. In the FG grade, only dimples are observed on the fracture surface. The fracture surface of the W1TiC and W2YO grades contains the trace of the deformation of grains, as well as the typical patterns of both intergranular and transgranular fracture modes are observed.

The fracture surface of W0.5ZC differs from all other products. At 300 °C and 400 °C, the surface contains several types of fracture patterns, including intergranular fracture, transgranular cleavage, dimples, deformation of grains, and delamination; however, dimples, deformation of grains, and delamination are only observed at the edges where the cracks initiated. Moreover, the percentage of intergranular fracture at 300 °C is higher than the one at 400 °C; intergranular fracture almost disappears on the fracture surface at 400 °C. With increasing the test temperature to 600 °C, the majority of the fracture changes and it contains dimples and delamination pattern.

4. Discussion

4.1. Mechanical properties

The product of UTS and uniform elongation reflects the amount of energy that can be accumulated in the material prior to the necking or plastic flow localization. The resistance to the occurrence of the plastic flow localization is directly connected to the strain hardening capacity. Materials with the large capacity exhibit longer uniform deformation as well as an elevation of the strength compared to the initial yield stress. The improved uniform deformation and high strength is also important for the good performance under fatigue condition. Thus, the material with the large uniform elongation and high strength is preferred for the application in the divertor PFC to sustain the thermal fatigue under the plasma discharge, to be coupled with the necessity to operate above the DBTT. The latter increases with the accumulation of the neutron irradiation dose. To this end, the operational temperature range with acceptable mechanical properties is defined by the DBTT and upper temperature above which the early necking onsets.

As shown in Fig. 5 c, each test material has a different suitable working temperature window. For example, W0.5ZC can be applied for

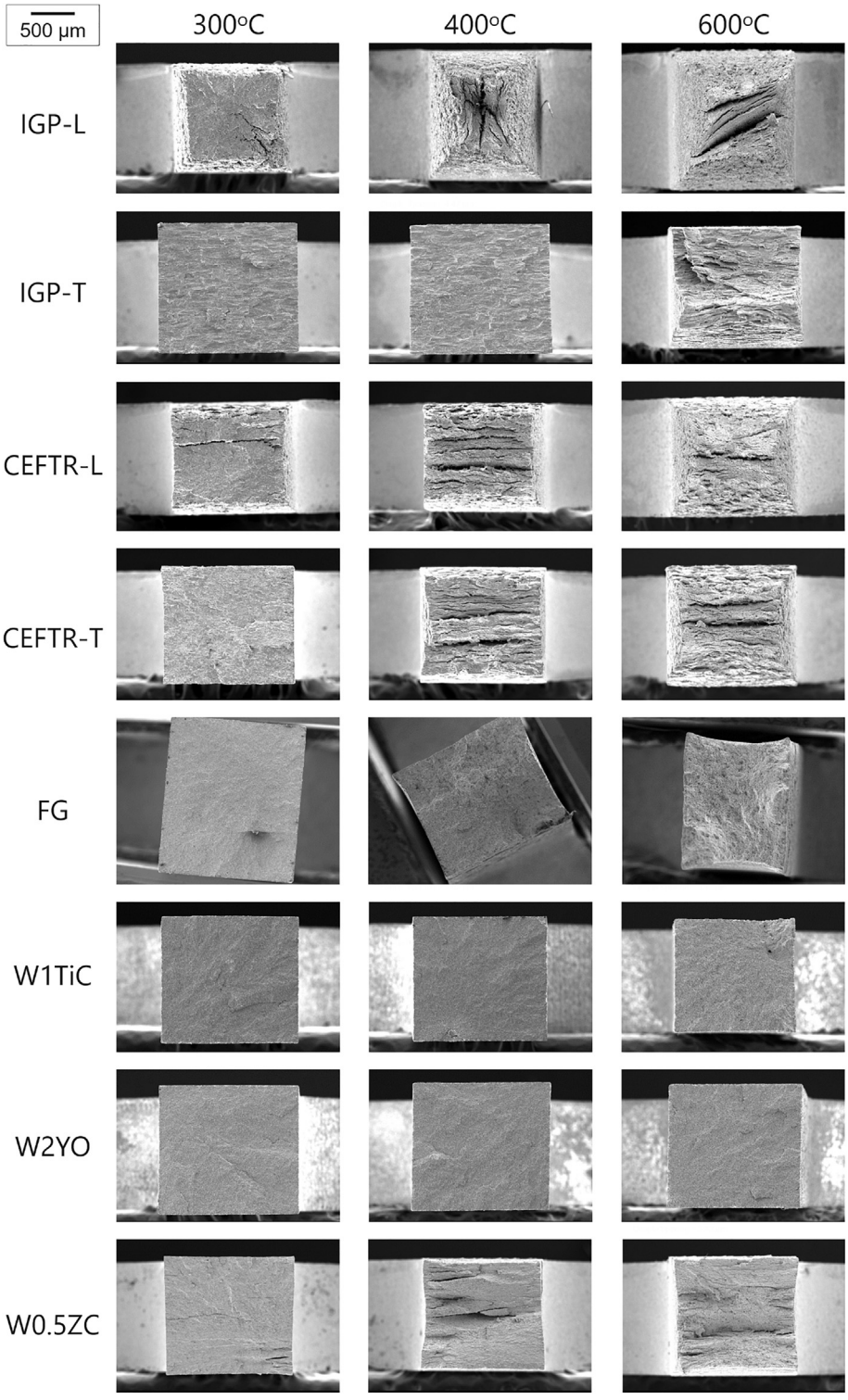

Fig. 6. Macroscopic appearance of fracture surface, as observed by SEM. The length scale bar, to be applied for all the micrographs, is depicted in the upper left corner.

the components working at low temperature, baseline W can operate in the medium temperature range, and W1TiC or FG can be used for the high-temperature components.

A product of FStrength and FStrain can be used to qualitatively indicate the material with the high resistance to fracture and crack propagation, hence high fracture toughness. A high toughness material can sustain high stresses and can experience significant plastic deformation before the fracture. However, the FStrength × FStrain value can only be used as an indicator since the actual fracture toughness will be proportional to the product of FStrength × FStrain × X_0, where X_0 is a characteristic microstructural length scale [23]. For instance, it can be the spacing between the particles that promote stress concentration accumulation and subsequent void damage prior to the development of the crack. Following the results of the microstructural analysis (see Fig. 7), the average dimple distance observed in the baseline W products (around 4–6 μm at 600 °C) is larger than that in the advanced W

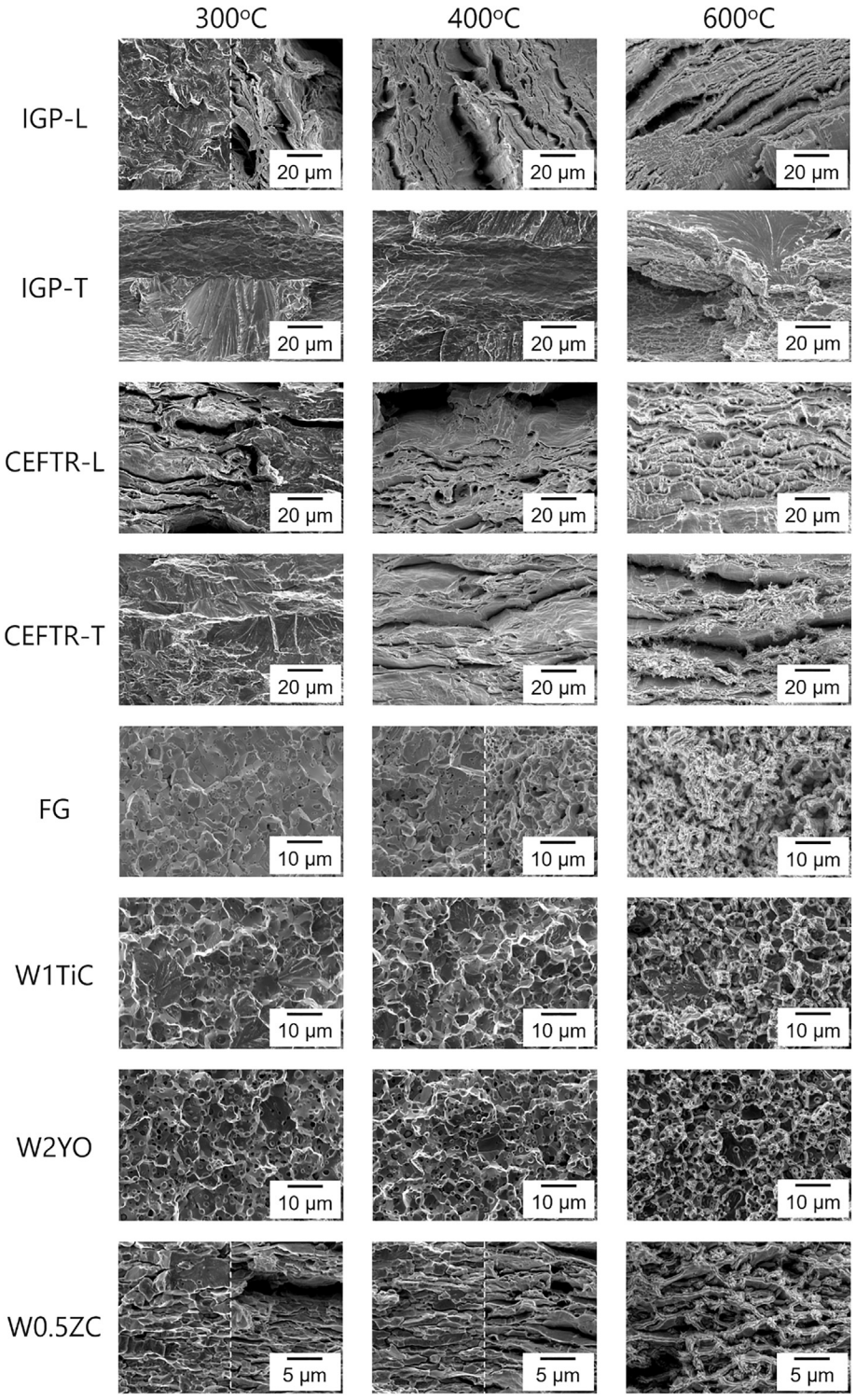

Fig. 7. High magnification of fracture surface, as observed by SEM.

materials (around 3–4 μm at 600 °C). Moreover, the average dimple spacing measured in the CEFTR-L (6.49 μm at 600 °C) is larger than in the IGP-L sample (4.90 μm at 600 °C). Thus, if one considers FStrength × FStrain × X_0 value as a measure of the fracture resistance, the baseline W product performs better than the advanced W materials. In particular, among the tested baseline W samples, the IGP-L sample has the best fracture resistance. It would be important to confirm this by the fracture toughness measurements.

4.2. Analysis of stress-strain response

Three types of the stress-strain deformation patterns were identified, namely: brittle (B), ductile (D), and early necking type (EN). B-type deformation corresponds to the fracture during the load in the elastic mode or just right after the yield point. D-type of deformation is the textbook curve of a ductile metallic material, which has a yield point, work hardening stage, ultimate tensile strength, and fracture limit. EN-type deformation refers to the case when necking occurs right

after the yield point but it is accompanied with considerable total post-necking elongation.

The materials, which have early necking at 600 °C, were produced by rolling or forging process, which implies texture, presence of elongated grains. This was less apparent for W0.5ZC due to the post-heat treatment but still present in some extent. According to our understanding, the main deformation mode in those materials is the in-grain plastic deformation; this kind of deformation by dislocation multiplication and glide is essentially limited by the small grain size. The inter-grain deformation occurs by the formation of dislocation pile-ups in front of GBs, they absorb by GBs and the newly formed dislocations move along the GBs. Note that transmission of dislocation slip between grains in the materials with strong texture and chaotic grain misorientation should be strongly suppressed. In such a picture, the GB triple junctions will act stress-concentrators where the nano-voids should nucleate and then coalescence. In turn, the nucleation and stress-driven coalescence of these voids would result in the reduction of the actual cross-section area of the sample being loaded under constant deformation rate. This would promote the formation of the necking region, and then the main plastic deformation would be concentration in the neck making the reduction of the ligaments even faster [24]. The reason why such flow softening behavior is promoted by increasing temperature is apparently due to the fact that thermal activation assists coalescence of voids in the temperature range where the transmission of plasticity between grain boundaries is still suppressed.

Table 2 summarizes the pattern of the stress-strain responses registered for the tested conditions. One can see that all tested materials can be sub-divided into two groups for which the trend, as the test temperature increases, is B-D-EN or B-EN. The materials of the former group are IGP-L, CEFTR-L, W0.5ZC, FG, W1TiC, and W2YO. On the other hand, IGP-T and CEFTR-T belong to the second group. This classification can also be observed from the plot showing the UTS and uniform elongation, presented in Fig. 8. As soon as the material operates above its DBTT, the uniform elongation increases with raising the test temperature and reaches its largest value at around DBTT + 100 °C. However, as temperature reaches around DBTT + 200 °C the uniform elongation starts to decrease. Clarification of this trend for the FG, W1TiC, W2YO materials requires additional tests at a higher temperature.

4.3. Baseline W

The results of the tensile tests for the commercial grades show that these materials exhibit early necking with increasing the test temperature irrespective of the load orientation. Below, we reconcile our explanation for the early necking in the L- and T-orientation of baseline W. In the case of L-orientation, the micro-cracks nucleate on the rough high angle grain boundaries, which oppose the transmission of piled dislocations into neighboring grains. Upon continuously applied load, the nucleated micro-crack begins to propagate until they get arrested by the elongated grain boundary interfaces. This results in the crack deflection and promotes intergranular fracture pattern [25,26]. Sustaining this deformation process requires input energy, and therefore

Table 2
Summary of classification of stress-strain curve.

	200 °C	300 °C	400 °C	600 °C
IGP-L	D	D	D	EN
IGP-T	B	B	B	EN
CEFTR-L	D	D	D	EN
CEFTR-T	B	B/EN	EN	EN
FG	B	B	D	D
W1TiC	B	D	D	D
W2YO	B	B/D	D	D
W0.5ZC	D	D	D	EN

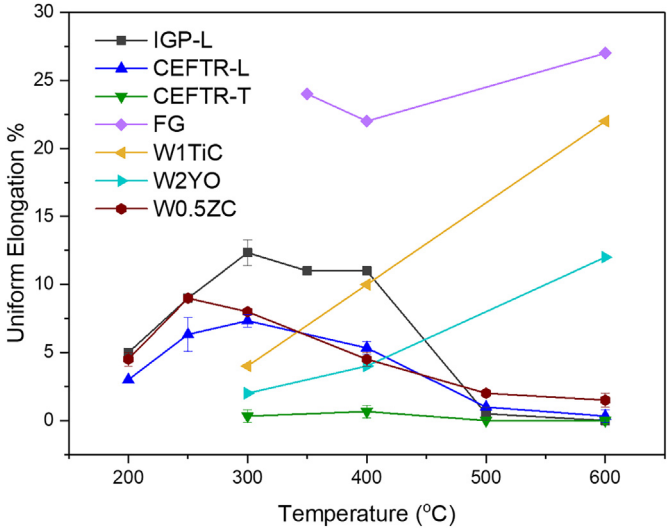

Fig. 8. The variation of uniform elongation with temperature.

material keeps undergoing macroscopic plastic deformation without significant loss of the engineering flow stress. As a result, a series of micro-cracks nucleate until they coalesce into a larger crack which defines the formation of the localized necking region. The numerous micro-cracks can be seen as delaminated grains all over the fracture surface, while few macro-cracks propagated across the whole fracture surface. Thus, the formation of numerous micro-cracks and their deflection by the elongated grains apparently delays the formation of the localized stress concentration resulting in the local necking region and eventual fracture. Macroscopically, such deformation results in the large post-necking elongation.

In the case of T-orientation, the grain interior available for the pile-up accumulation is smaller. As soon as the resolved shear stress is high enough to activate dislocation glide, the pile-ups will establish stress concentration near grain boundaries; this phenomenon will generate micro-cracks in a similar way as for the deformation mechanism of the samples with L-orientation. But since the elongated grains are parallel to the direction of crack propagation, the crack deflection distance is much smaller. Thus, the propagation of such micro-cracks should be much faster as compared to the situation in the L-orientation load. Correspondingly, the strain localization happens shortly after the yield point, and total elongation is also reduced, as compared to the results obtained for the L-orientation sample.

4.4. Advanced W

It is well known that the strength of the materials is defined by the properties of the weakest links available. Usually, it is grain boundary interface which causes the accumulation of stress concentration by the dislocation pile-up formation. Thus pile-ups can dissolve by transmission through or absorption by grain boundaries. In the latter case, the absorbed bulk dislocations are converted into grain boundary dislocations (which produce grain boundary sliding, respectively). Segregation of impurities to grain boundary interfaces can further suppress plasticity by obstructing movement of grain boundary dislocations. Thus, the grain boundary which accumulated a large fraction of interstitial impurities (like carbon, nitrogen or oxygen) tend to be prone to an intergranular fracture failure. However, as indicated by Gludovatz et al. [27], the impurities on grain boundaries have limited influence on fracture behavior at a test temperature below DBTT. Thus, the fracture behavior can be used as an indication of the purity/cleanness of grain boundaries from interstitial impurities, based on tests done above DBTT.

The fracture surface of the FG grade contains a high fraction of

transgranular fracture. It indicates that most of the grain boundaries are free from impurities. Moreover, FG grade had the highest DBTT among the lab grades studied here. The limited porosity found in the FG material, as observed on the EBSD maps, might be the reason of the high DBTT measured from the tests, since large number of micro-voids should act as nuclei for stress concentration regions. As a result, the FG samples fractured without any plastic deformation below 400 °C. However, the porosity can be considerably reduced by advanced heat treatment and improved sintering procedure, as preliminary tests have already shown.

The fracture surface of the W1TiC and W2YO grades showed the presence of the micrometer size particles, located on the grain boundaries, which is in line with results of Antusch et al. [28]. The particles on grain boundaries also will introduce suppression of the grain-boundary plastic deformation provoking stress concentration. Thus, these materials exhibit a relatively small total elongation below 400 °C. However, the TiC particles strengthen the grain boundaries and therefore shift the temperature for the onset of the early necking deformation [29–31]. The microstructural analysis has shown that the W1TiC grade had a higher grain boundary coherency compared to W2YO, which is in line with the higher fraction of transgranular fracture observed in W1TiC material. Therefore, at elevated temperature, large uniform elongation was recorded in the W1TiC samples.

In the microstructure of non-deformed materials, we did not observe pores except in the FG grade. The original work describing the development of W1TiC and W2YO grades indicates that Ti and Y elements, detected by the Auger electron spectroscopy (AES), are present in the pores of the fracture surface [28]. Thus, the pores on the fracture surface of W1TiC and W2YO observed here might be the left-out of the carbide or oxide particles. Also, in the fractured grains of W0.5ZC at 300 °C and 400 °C, micro-pores are observed (see Fig. 7), these pores might be the left-outs of ZrC particles, nearly distributed in the W grains as mentioned in the original work [16].

Following the comparative EBSD analysis, W0.5ZC have the most coherent grain boundary patters as compared to other studied here grades. This grain boundary coherency should reduce the resistance (as compared to other grades tests) for the permeation/absorption of dislocations through/by grain boundaries. That is probably why rather low work hardening is observed for the W0.5ZC 400 °C. Yet thanks to nano-sized ZrC, the achieved grain refinement apparently enables both high yield strength and low DBTT at the same time. The limited size of ZrC particles ensures stability and fine structure of grain boundary interfaces and at the same time does not suppress the inter-granular plasticity. In the original work [16], it is noted that Zr acts as an oxygen gatherer, which “cleans” the grain boundaries. As observed from the fracture surface of W0.5ZC, the majority of the fracture grains showed transgranular feature, which also support the conclusion on low impurity concentration at grain boundaries. W0.5ZC also shows early necking at 600 °C but with smaller post-necking elongation. In the following, we construct our explanation. The grains of W0.5ZC are less elongated and nearly equiaxed. Therefore, the transmission of dislocation slip between grains is only weakly suppressed; the transmission of dislocation slip coupled with the coherency grain boundaries results in larger uniform elongation compared with commercial W at 600 °C. However, the coalescence of voids is promoted by the increasing temperature; and these voids reduce the actual cross-section. Thus, the result is early necking.

Relatively high DBTT of FG, W1TiC, and W2YO materials, as compared to the fine-grain W0.5ZC grade, should probably be attributed to the mis-ordered structure of grain boundary interfaces, porosity, and presence of large-size particles at the grain boundary interfaces (in PIM-produced grades). However, as FG operates above DBTT, thanks to the presence of initially low dislocation density and refined grain interfaces (both invoked by the high temperature sintering), the large uniform elongation and work hardening capacity are ensured by the multiplication of dislocations and transgranular slip [32]. On the other hand, we suspect that the transgranular slip is reduced in the PIM-based W grades because of the high density of precipitates, which increase the flow stress but suppress the plasticity in the grain boundary region.

5. Conclusions

In this work, two commercially available W grades and several lab-scale recently developed grades were tested in the temperature range 150–600 °C using miniaturized tensile sample geometry. The main purpose of the work was to reveal the threshold temperature for ductile plastic deformation as well as to clarify the features of the fracture mechanisms in the ductile regime. Based on the obtained results and discussions it is possible to state the following:

A. Commercial IGP and CEFTR products, tested in L direction, have considerable uniform elongation in the temperature range 300–400 °C, which depends on the texture and initial microstructure. Although W0.5ZC also has large uniform elongation at 250 °C and 300 °C, the uniform elongation gradually reduces with increasing temperature. Important to note that IGP, tested in L direction, has the highest fracture resistance out of all tested materials. While, the W0.5ZrC has the lowest DBTT (around 100 °C), as indicates in the original work [16], and still sustains rather high yield strength at 600 °C.
B. The lab-scale FG, W1TiC, W2YO grades exhibit relatively high DBTT, above 300 °C, however, these materials show large uniform elongation and capacity for work hardening up to 600 °C, and likely even higher.
C. Overall, each tested material exhibits brittle-ductile-early necking deformation behavior as the test temperature rises. The ductile behavior and capacity for work hardening are preserved over a limited temperature range, which extends by about 300° above the DBTT, as was revealed for the IGP-L, CEFTR-L and W0.5ZC. Clarification of the value for this temperature range for the FG, W1TiC, W2YO grades requires additional tests at a higher temperature.
D. The presence of texture in the commercial grades has an impact on the above discussed Brittle/Ductile/Early Necking trend. In particular, for both IGP and CEFTR grades tested in T-orientation, the observation indicates the direct transition from brittle to early necking deformation pattern without attaining the ductile deformation with somewhat considerable uniform elongation.
E. The fracture surface analysis indicates that the commercial grades tend to delaminate at high temperature. On the other hand, the fracture surface of the lab-scale grades mainly consists of trans/inter-granular fracture. Worth to note that W0.5ZC revealed all types of fracture, where the fraction of each type of pattern depends on the test temperature.

Acknowledgement

This work has been carried out within the framework of the EUROfusion Consortium and has received funding from the Euratom Research and training programme 2014–2018 under grant agreement No. 633053. Part of the work was also supported by Czech Science Foundation grant No. 17-23154S. The views and opinions expressed herein do not necessarily reflect those of the European Commission.

Reference

[1] D. Stork, P. Agostini, J.L. Boutard, D. Buckthorpe, E. Diegele, S.L. Dudarev, et al., Developing structural, high-heat flux and plasma facing materials for a near-term DEMO fusion power plant: the EU assessment, J. Nucl. Mater. 455 (2014) 277–291.
[2] D. Maisonnier, I. Cook, S. Pierre, B. Lorenzo, D.P. Luigi, G. Luciano, et al., DEMO and fusion power plant conceptual studies in Europe, Fusion Eng. Des. 81 (2006) 1123–1130.
[3] G. Federici, W. Biel, M.R. Gilbert, R. Kemp, N. Taylor, R. Wenninger, European DEMO design strategy and consequences for materials, Nucl. Fusion 57 (2017).

[4] G. Pintsuk, Tungsten as plasma facing material, Compr. Nucl. Mater. 4 (2012) 551–581.
[5] C. Linsmeier, M. Rieth, J. Aktaa, T. Chikada, A. Hoffmann, J. Hoffmann, et al., Development of advanced high heat flux and plasma-facing materials, Nucl. Fusion 57 (2017).
[6] H. Noto, S. Taniguchi, H. Kurishita, S. Matsuo, T. Ukita, K. Tokunaga, et al., Effect of grain orientation and heat treatment on mechanical properties of pure W, J. Nucl. Mater. 455 (2014) 475–479.
[7] H. Sheng, G. Van Oost, E. Zhurkin, D. Terentyev, V.I. Dubinko, I. Uytdenhouwen, et al., High temperature strain hardening behavior in double forged and potassium doped tungsten, J. Nucl. Mater. 444 (2014) 214–219.
[8] G. Pintsuk, I. Uytdenhouwen, Thermo-mechanical and thermal shock characterization of potassium doped tungsten, Int. J. Refract. Met. Hard Mater. 28 (2010) 661–668.
[9] B. Gludovatz, S. Wurster, A. Hoffmann, R. Pippan, Fracture toughness of polycrystalline tungsten alloys, Int. J. Refract. Met. Hard Mater. 28 (2010) 674–678.
[10] J. Reiser, S. Wurster, J. Hoffmann, S. Bonk, C. Bonnekoh, D. Kiener, et al., Ductilisation of tungsten (W) through cold-rolling: R-curve behaviour, Int. J. Refract. Met. Hard Mater. 58 (2016) 22–33.
[11] S. Wurster, R. Pippan, Miniaturized cantilever bending experiments for determination of fracture properties of tungsten as a model material, Determination of Mechanical Properties of Materials by Small Punch and Other Miniature Testing Techniques, 2nd International Conference Sstt, 2012, pp. 271–275.
[12] J.W. Coenen, S. Antusch, M. Aumann, W. Biel, J. Du, J. Engels, et al., Materials for DEMO and reactor applications-boundary conditions and new concepts, Phys. Scr. T167 (2016).
[13] M. Rieth, A brief summary of the progress on the EFDA tungsten materials program, J. Nucl. Mater. 442 (2013) S80–S173.
[14] J. Riesch, Y. Han, J. Almanstotter, J.W. Coenen, T. Hoschen, B. Jasper, et al., Development of tungsten fibre-reinforced tungsten composites towards their use in DEMO-potassium doped tungsten wire, Phys. Scr. T167 (2016).
[15] L.H. Zhang, Y. Jiang, Q.F. Fang, Z.M. Xie, S. Miao, L.F. Zeng, et al., Microstructure and mechanical properties of tungsten composite reinforced by fibre network, Front. Mater. Sci. 11 (2017) 190–196.
[16] Z.M. Xie, R. Liu, S. Miao, X.D. Yang, T. Zhang, X.P. Wang, et al., Extraordinary high ductility/strength of the interface designed bulk W-ZrC alloy plate at relatively low temperature, Sci. Rep. (2015) 5 UK.
[17] P. Jung, A. Hishinuma, G. Lucas, H. Ullmaier, Recommendation of miniaturized techniques for mechanical testing of fusion materials in an intense neutron source, J. Nucl. Mater. 232 (1996) 186–205.
[18] A. Kohyama, K. Hamada, H. Matsui, Specimen size effects on tensile properties of neutron-irradiated steels, J. Nucl. Mater. 179 (1991) 417–420.
[19] Y. Zhao, Y. Guo, Q. Wei, T. Topping, A. Dangelewicz, Y. Zhu, et al., Influence of specimen dimensions and strain measurement methods on tensile stress–strain curves, Mater. Sci. Eng. A 525 (2009) 68–77.
[20] Y. Zhao, Y. Guo, Q. Wei, A. Dangelewicz, C. Xu, Y. Zhu, et al., Influence of specimen dimensions on the tensile behavior of ultrafine-grained Cu, Scr. Mater. 59 (2008) 627–630.
[21] R. Lowrie, A. Gonas, Single-crystal elastic properties of tungsten from 24° to 1800 °C, J. Appl. Phys. 38 (1967) 4505–4509.
[22] Z. Yuan, F. Li, P. Zhang, B. Chen, F. Xue, Mechanical properties study of particles reinforced aluminum matrix composites by micro-indentation experiments, Chin. J. Aeronaut. 27 (2014) 397–406.
[23] T. Pardoen, J. Hutchinson, Micromechanics-based model for trends in toughness of ductile metals, Acta Mater. 51 (2003) 133–148.
[24] D. Lassance, D. Fabregue, F. Delannay, T. Pardoen, Micromechanics of room and high temperature fracture in 6xxx Al alloys, Prog. Mater. Sci. 52 (2007) 62–129.
[25] D. Rupp, R. Mönig, P. Gruber, S. Weygand, Fracture toughness and microstructural characterization of polycrystalline rolled tungsten, Int. J. Refract. Met. Hard Mater. 28 (2010) 669–673.
[26] E. Gaganidze, D. Rupp, J. Aktaa, Fracture behaviour of polycrystalline tungsten, J. Nucl. Mater. 446 (2014) 240–245.
[27] B. Gludovatz, S. Wurster, T. Weingärtner, A. Hoffmann, R. Pippan, Influence of impurities on the fracture behaviour of tungsten, Philos. Mag. 91 (2011) 3006–3020.
[28] S. Antusch, D.E. Armstrong, T.B. Britton, L. Commin, J.S.-L. Gibson, H. Greuner, et al., Mechanical and microstructural investigations of tungsten and doped tungsten materials produced via powder injection molding, Nucl. Mater. Energy 3 (2015) 22–31.
[29] H. Kurishita, Y. Amano, S. Kobayashi, K. Nakai, H. Arakawa, Y. Hiraoka, et al., Development of ultra-fine grained W–TiC and their mechanical properties for fusion applications, J. Nucl. Mater. 367 (2007) 1453–1457.
[30] M. Kajioka, T. Sakamoto, K. Nakai, S. Kobayashi, H. Kurishita, S. Matsuo, et al., Effects of plastic working and MA atmosphere on microstructures of recrystallized W–1.1% TiC, J. Nucl. Mater. 417 (2011) 512–515.
[31] H. Kurishita, S. Matsuo, H. Arakawa, M. Narui, M. Yamazaki, T. Sakamoto, et al., High temperature tensile properties and their application to toughness enhancement in ultra-fine grained W-(0-1.5) wt% TiC, J. Nucl. Mater. 386 (2009) 579–582.
[32] A.F. Liu, Mechanics and Mechanisms of Fracture: An Introduction, ASM International, 2005.